Journal of Pain Research

Dovepress
open access to scientific and medical research

Open Access Full Text Article

ORIGINAL RESEARCH

Analysis of Ionomic Profiles of Spinal Cords in a Rat Model with Bone Cancer Pain

Jinlu Huang[1,*], Jiugeng Chen[2,*], Le Ma[3,*], Xieyi Zhu[4], Lili Wan[1], Xinyan Li[4], Cheng Guo[1]

[1]Department of Pharmacy, Shanghai Sixth People's Hospital Affiliated to Shanghai Jiao Tong University School of Medicine, Shanghai, People's Republic of China; [2]Instrumental Analysis Center, Shanghai Jiao Tong University, Shanghai, People's Republic of China; [3]Department of Pharmacy, Shanghai Jiao Tong University School of Medicine, Shanghai Mental Health Center, Shanghai, People's Republic of China; [4]College of Pharmacy, Shanghai Jiao Tong University, Shanghai, People's Republic of China

*These authors contributed equally to this work

Correspondence: Xinyan Li; Cheng Guo, Email lixy@sjtu.edu.cn; guopharm@126.com

Background: Ionomics is used to study levels of ionome in different states of organisms and their correlations. Bone cancer pain (BCP) severely reduces quality of life of patients or their lifespan. However, the relationship between BCP and ionome remains unclear.

Methods: The BCP rat model was constructed through inoculation of Walker 256 cells into the left tibia. Von Frey test, whole-cell patch-clamp recording and inductively coupled plasma mass spectrometry (ICP-MS) technologies were conducted for measuring tactile hypersensitivity, the frequency and amplitude of miniature excitatory postsynaptic currents (mEPSCs) of neurons of spinal slices, and ionome of spinal cord samples, respectively. Principal component analysis (PCA) was used to explore ionomic patterns of the spinal cord.

Results: The BCP rat model was successfully constructed through implantation of Walker 256 cells into the left tibia. The frequency and amplitude of mEPSCs of neurons in the spinal cord slices from the BCP model rats were notably greater than those in the sham control. In terms of ionomics, the spinal cord levels of two macroelements (Ca and S), four microelements (Fe, Mn, Li and Sr) and the toxic element Ti in the BCP group of rats were significantly increased by inoculation of Walker 256 cancer cells, compared to the sham control. In addition, the correlation patterns between the elements were greatly changed between the sham control and BCP groups. PCA showed that inoculation of Walker 256 cells into the tibia altered the overall ionomic profiles of the spinal cord. There was a significant separation trend between the two groups.

Conclusion: Taken together, inoculation of Walker 256 cells into the left tibia contributes to BCP, which could be closely correlated by some elements. The findings provided novel information on the relationship between the ionome and BCP.

Keywords: bone cancer pain, spinal cord, micronutrient, ionomic profile

Introduction

Bone cancer pain (BCP) is a kind of complex and unique alagesic state sharing partial pathological characteristics with inflammatory and neuropathic pain. 75–90% of advanced patients with tumor metastasis into bones experience BCP.[1,2] It is reported that more than 44% of cancer patients still suffer from insufficient relief of pain through the currently available therapeutic medicines.[3] Furthermore, BCP often results in depression, anxiety and even cognitive dysfunction, which severely reduce the quality of life of patients and even affect their lifespan. In order to effectively relieve, even control BCP and improve their quality of life, it is very essential to innovate pharmacotherapies, which are based on completely deciphering its pathogenesis. For the purpose, dozens of models of BCP have been successfully established in rats and mice over the past decades.[4] A growing number of findings obtained in these models have revealed that some critical genes,[5] RNAs,[6–8] peptides/protein (e.g., calcitonin gene-related peptide, neuropeptide Y, PI3K/Akt)[9–11] and small biochemical molecules (e.g., D-serine, glycine)[12,13] in the spinal cord were complicatedly involved in BCP through a variety of mechanisms, including central sensitization, oxidative stress, neuroinflammation, glial cell activation,

Received: 1 November 2023
Accepted: 4 April 2024
Published: 23 April 2024

mitochondrial dysfunction and others.[11,14–17] However, BCP is still a major clinical challenge due to its potential unclear pathologic mechanisms.

The ionome in an organism is defined as a set of inorganic elemental and mineral nutrient compositions,[18] which play pivotal roles in the health of human beings and animals, because they are essential in modulating DNA repair, protein synthesis, metabolic homeostasis, immune regulation, anti-inflammatory responses and antioxidant defense. Some of them in ionome function as cofactors of enzyme activity (e.g., iron [Fe], zinc [Zn], copper [Cu]), stabilizers of genes or protein structure and function (e.g., magnesium [Mg], sulfur [S], Zn, Cu), components of skeletons (e.g., calcium [Ca], phosphorus [P], Mg), modulators of organic (whole body or cell) acid-base and electrolyte balance (e.g., sodium [Na], potassium [K]), second messengers (e.g., Ca), dependent participants of ferroptosis (e.g., Fe) and cuproptosis (e.g., Cu), as well as components of redox reactions (e.g., Zn, selenium [Se], manganese [Mn]).[18–20] Excessive accumulation of elements and minerals as well as their deficiency might be the most significant risk factors for lots of diseases, such as autism spectrum disorders (ASD),[21] Alzheimer's disease,[22] diabetes and insulin resistance,[23] revealing that their imbalance of ionome may involve in the pathogenesis of the corresponding diseases. Interestingly, emerging findings have suggested that some elements (e.g., Zn, Mg) are intricately linked to hyperalgesia.[24,25] Ferroptosis, a novel Fe-dependent manner of cell death, is also involved in inflammation,[26] neuropathic pain,[27] morphine tolerance[28] and BCP (our unpublished data). The evidence above implies changes in ionome might systemically involve into the process of formation and maintenance of pain. It is argued that studies focusing on the effects of a single element on hyperalgesia may have shortcomings, and may not provide enough information to analyze direct or indirect correlation between elements in BCP. The production of some ions also affects others. Therefore, it is very important to analyze the ionome at the same time.

Ionomics is the study of ionome. It is a high-throughput approach and its major purpose is to measure the levels of elements and minerals in a biological system in different states, and to further elucidate their correlations. It has been well qualified as an emerging research field following genomics, proteomics and metabolomics. Unlike the other omics, ionomics has been widely applied in environmental and botanic studies for dozens of years.[29–31] Recently, in light of important roles of elements and minerals as micronutrients in human health and diseases, ionomics has been extensively used to research their distribution, metabolism and interactions under different pathophysiological states,[32,33] which provides a useful strategy for exploring novel ionome-based mechanisms of diseases and seeking biomarkers of diagnosis and prognosis evaluation. In addition, ionomics may contribute to not only understanding gene or protein networks that affect the ionome balance, but also providing possible recipes for prevention or treatment of some complex diseases.[34] Moreover, each type of disease has a distribution trait of ions in tissue samples from patients, which might serve as potential indicators for the respective disease. The ionome imbalance may reflect broader disruption in human health and nutrition.[18] Identification and quantification of differential iomone in the spinal cord may help us better understand the mechanisms of BCP and how it occurs and develops. Obviously, it is very important to elucidate the relationship between BCP and the metabolism and homeostasis of ionome, which still remains unclear. Therefore, the study aims to identify and analyze ionomic profiles of the spinal cord of model rats with BCP induced by inoculation of Walker 256 cancer cells into left tibia and their internal relationships.

Methods

Cells and Animals

Walker 256 rat mammary gland carcinoma cells were kindly provided by Prof. Ling Xu (LongHua Hospital Shanghai University of Traditional Chinese Medicine, Shanghai, China). The use of Walker 256 cells in the study was approved by the Research Ethics Committee of Shanghai Municipal Sixth People's Hospital. The cells (2×10^7) suspended in 1 mL of aseptic PBS solution were injected into the abdominal cavity of female SD rats (50–60 g) which were purchased from Shanghai Experimental Animal Institute for Biological Sciences (Shanghai, China). Seven days later, cells were collected from the above rats under sterile conditions. To prepare the BCP model, adult female SD rats (150–180 g) were also purchased from Shanghai Experimental Animal Institute for Biological Sciences (Shanghai, China). All rats were fed under controlled conditions at a temperature of 22 ±2 °C and relative humidity of 55±15% with a 12-h light-dark cycle. Normal food and water were provided daily *ad libitum* to the rats. Standard chow diet for lab animals was purchased from Jiangsu Xietong Bioengineering Co. Ltd. (Nanjing, China). They

were acclimatized to the lab environment for 7 days before all the experiments were carried out. All the experimental work was in accordance with an approved protocol issued by the Animal Care and Welfare Committee of Shanghai Municipal Sixth People's Hospital. The animal experiments strictly adhered to the National Institutes of Health Guide for Care and Use of Laboratory Animals (Publication No. 80–23, revised 1996).

Preparing the BCP Rat Model

The BCP rat model was prepared as previously described.[12] Briefly, Walker 256 cells (4×10^5) in 10 μL of sterile PBS solution in a 50 μL microinjection syringe were directly implanted into the left tibia cavity of rats fully anesthetized with 10% chloral hydrate at a concentration of 300 mg/kg. The injection holes were sealed with aseptic bone wax to avoid the spread of the cells to surrounding tissues. In the sham group of rats, the same operation except only injection of PBS without cancer cells was performed. After surgery, all the animals were put back into their cages for recovery from anesthesia.

Measuring Paw Withdrawal Thresholds

Paw withdrawal thresholds (PWTs) of the ipsilateral hindlimbs of the sham and BCP groups of rats were measured on the 2nd, 5th, 10th, 14th days after surgery, respectively, as previously described in detail elsewhere.[12] Briefly, rats were placed on mechanical allodynia test equipment covered with plastic boxes and in the detecting environment for at least 30 min before beginning the mechanical behavioral test. The PWTs of the ipsilateral hindpaws of rats were assessed using 2290 CE electronical Von Frey filaments (IITC Life Science, Woodland Hills, CA, USA) with a force ranging from 0.1 to 90 g. The filament was slightly applied to the left foot pad with gradually increasing force until the rat suddenly withdrew the hindpaw. The minimal force value evoking a withdrawal response was considered the nociceptive threshold.[35] The PWTs of the ipsilateral hindpaws of all rats were evaluated three times with a 10-min interval.

Micro-Computed Tomography Scans for Tibiae

The bilateral tibia tissue samples from rats with BCP on the 14th day post inoculation of cancer cells into left tibiae were procured and preserved in ethanol for performing micro-computed tomography (μCT) scans. Scans were carried out at 35*35*35 μm voxel size, 65 kV, 385 μA and 0.55° rotation step (180° angular range) using SkyScan-1176 μCT (Bruker Corporation, Belgium) system. And photos were observed with the DataViewer software (1.5.4.0 version, Bruker Corporation, Belgium).

Whole-Cell Patch Clamp Recording

Slices for electrophysiological assessments were prepared from segregated spinal cord lumbar enlargement of rats that were anesthetized with inhaled isoflurane and killed through decapitation, as described elsewhere.[13,35] Briefly, lumbar spinal cords were quickly collected and put in ice-cold oxygenated high sucrose cutting solution: 234 mM sucrose, 3.6 mM KCl, 1.2 mM $MgCl_2$, 1.2 mM NaH_2PO_4, 12 mM glucose, 2.5 mM $CaCl_2$ and 25 mM $NaHCO_3$ for 90 s. The 400-μm thick spinal cord slices were prepared by using a Leica VT-1200S vibratome (Leica Biosystems, Wetzlar, Germany). Whole-cell patch-clamp recording was carried out in the ipsilateral dorsal horn neurons of the substantia gelatinosa with a 4–5 MΩ pipette (Sutter Instruments, Novato, CA, USA) with inner and outer diameters of 0.5 and 1.0 mm, respectively. All neurons were clamped at −70 mV. The excitability of spinal cord lamina II neurons was recorded in both the sham and BCP groups of rats for 5 min with Axon Axopatch 200B amplifier (Molecular Devices, LLC. CA, USA). The cumulative distribution plots for miniature excitatory postsynaptic current (mEPSC) amplitude and interevent intervals were calculated by Clampfit software version 10.7 (Molecular Devices, LLC. CA, USA).

Element Detection

Samples of the spinal cord were immediately isolated and collected after the sham control and BCP groups of rats were killed on the 14th day post surgery, as described previously.[13,36] Briefly, the spinal cord tissues were quickly separated on ice and weighted following slight removal of their membranes. Then, in a dedicated trace element clean room equipped with a Class 100 clean hood, all the samples were digested in 2 mL of 69% nitric acid at 120 °C in a 50 mL metal-free

tube on the digestion block (DigiPREP Jr., SCP-Science, Quebec, Canada) for approximately 1 h until the tissue had almost disappeared. During incubation, the tubes were gently swirled every 20 min. When the samples had cooled, 0.5 mL of H_2O_2 was added and the samples were heated at 120 °C for another 30 min. After digestion was complete, the tubes were cooled to room temperature and the volume was brought up to 20 mL with ultrapure water. Calibration standards were prepared by diluting 1000 mg/L ICP-MS standard solutions (Spex CertiPrep, Metuchen, NJ, America) with 10% nitric acid. Elements were detected using inductively coupled mass spectrometry (ICP-MS, NexION2000G, PerkinElmer, CA, USA), and element concentrations were calculated using external calibration and Rh as an internal standard. A certified reference standard (T07243QC, FAPAS, America) was used for quality control.

Data Statistical Analysis

GraphPad Prism 9.0 software (GraphPad Software Inc., San Diego, CA, USA) was used for data statistics. The data are expressed as the mean ± SEM. The statistical significance *p* value was set at 0.05. The data were analyzed by two-way repeated measures ANOVA or unpaired and two-tailed Student's *t*-test. The analytical method of Pearson's correlation coefficient, which is the test statistic that measures the statistical relationship between two continuous variables, was introduced in this study. Correlations among continuous variables of elements were analyzed using SPSS 21.0 (IBM, Chicago, IL, USA). Bivariate (by Pearson's correlation test) analysis was performed to estimate the associations between continuous variables. Principal component analysis (PCA) was carried out with Origin 2021 version software (OriginLab Corporation, Northampton, USA).

Results

Morphological Observation and Behavioral Assessment of Mechanical Hyperalgesia/Allodynia in Rats with Bone Cancer

By day 14 after inoculation of Walker 256 cancer cells into the tibia of the left hindlimb, morphological observation revealed clear intumescentia around the ipsilateral tibiae in the cancer-bearing rats, in contrast to both the sham control rats and the contralateral ones of the same model rats. Next, we assessed the time course of mechanical hyperalgesia/allodynia in the rat model with BCP induced by Walker 256 cancer cells. During the 14-day observation period, the rats bearing Walker 256 cancer cells experienced gradually lower ipsilateral PWTs to innocuous mechanical stimulus in a time-dependent manner, compared to the control group of the rats with sham operation. The results indicated that BCP was progressively strengthened in the rat model, reached the lower PWTs (14.8±1.8 g) on the 10th day after operation, compared to the corresponding sham control group (24.8±1.8 g). It remained for at least 14 days. The time course of mechanical hyperalgesia/allodynia in rats with BCP is shown in Figure 1. The validation of the BCP rat model was also executed with μCT scans for the bilateral tibiae of BCP rats. μCT scanning imaging showed that there was significant bone destruction in the ipsilateral tibia on the 14th day after inoculation of cancer cells, compared to the contralateral one of the same BCP rat, as shown in Figure S1. The data suggested that the bone structures of ipsilateral tibiae in BCP rats were abnormally eroded and destroyed by active tumor cells.

Changes in Ipsilateral Neuronal mEPSCs in Spinal Dorsal Horns of BCP Rats

Next, to clarify changes in excitatory synaptic transmission in spinal cords on the 14th day after surgery, the whole-cell recordings of mEPSCs as inward currents were performed in neurons of the ipsilateral dorsal horn in spinal cord slices derived from the sham control and BCP rats. The electrophysiological findings showed that the frequency and amplitude of mEPSCs in BCP rats was notably greater than those in the sham control rats, as shown in Figure 2A. The curves of the cumulative distribution of amplitude and inter-event interval of mEPSCs were shifted to the right (Figure 2B) and left (Figure 2C) in the BCP group, compared to the sham control rats, respectively. The analysis of data indicated that amplitude (Figure 2D) and frequency (Figure 2E) of mEPSCs were significantly increased in the BCP group, in contrast to the sham control group. These data from patch-clamp recordings of neurons also suggested that allodynia of rats was successfully induced by inoculation of Walker 256 cancer cells into the left tibia.

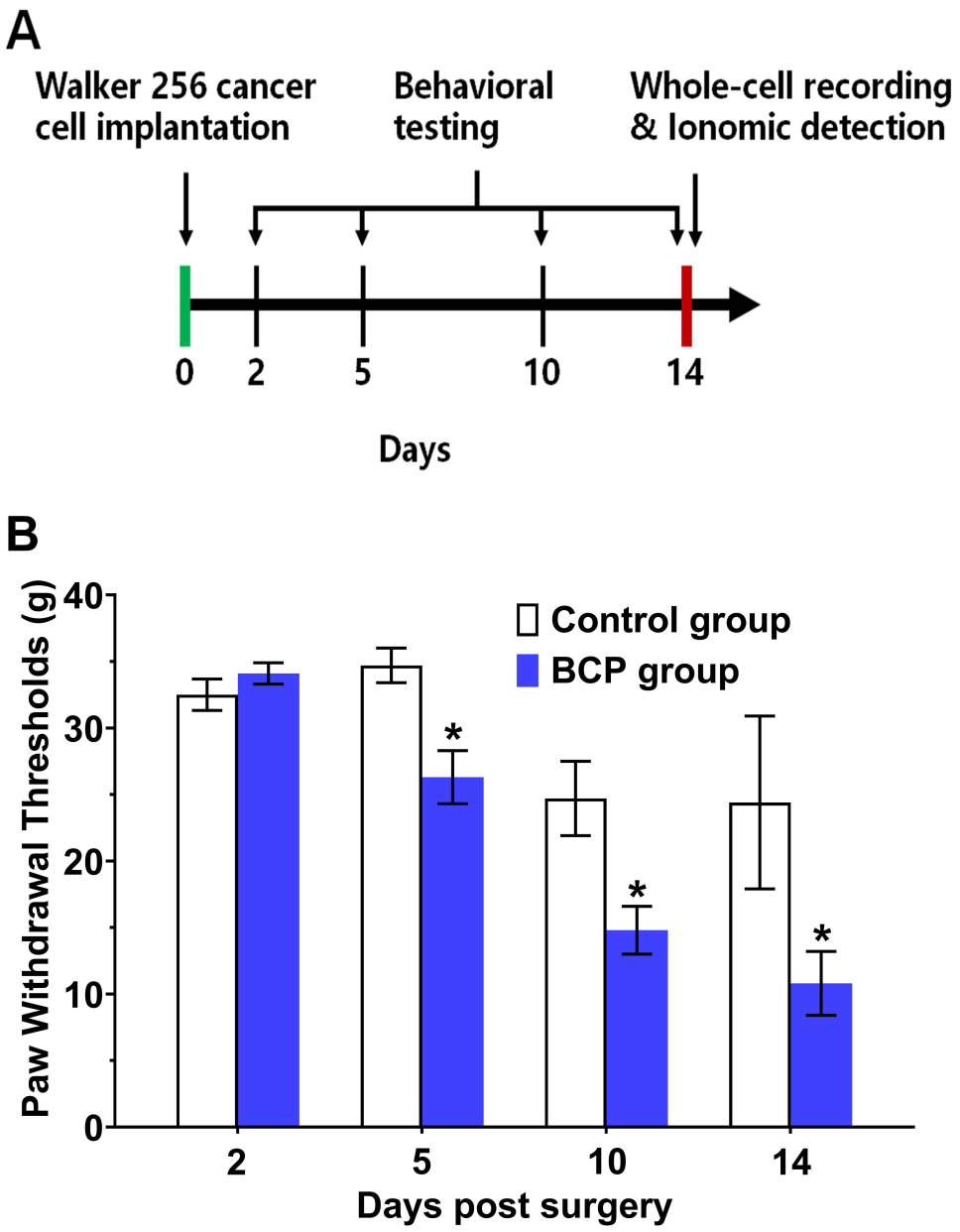

Figure 1 Preparation of the rat model with BCP, the assessment of their hyperalgesic/allodynic behaviors. (**A**) Schematic diagram of the study: Following acclimation of environment for rats, implantation of Walker 256 cancer cells into the left tibia of their hindlimbs to prepare BCP model. The hyperalgesic/allodynic testing was carried out on the 2nd, 5th, 10th, 14th days post-surgery. The spinal cord samples were collected for the whole-cell recording and ionomic detection. (**B**) Changes in the ipsilateral PWTs on the 2nd, 5th, 10th, 14th days after surgery in the sham control and BCP groups of rats. Significant changes are denoted with an asterisk, compared to the corresponding control group of rats (n = 5–12, *p<0.05).

Changes in the Levels of Ionome in the Spinal Cord in the Rats with BCP

To explore changes in ionome levels of the spinal cord, the spinal cord samples of the sham and BCP groups of rats were slightly separated and rapidly collected on the 14th day after injection of Walker 256 cancer cells into the left tibia. The contents of 23 elements of all the samples were examined through applying ICP-MS ionomic analytical procedures.

Therein, the spinal cord contents of four macroelements (Na, K, Ca, P) were milligram levels per gram of tissues, which were markedly higher than those of others (microgram or lower levels per gram of tissues) in both the sham control group and BCP model group. And it was also displayed that the content of the element P in the spinal cord was the highest among the detected elements, up to about 3.20 mg per gram tissue. Among the six macroelements (Na, K, Ca, Mg, S, P), the spinal cord levels of the elements Ca (1.47 fold, p = 0.037) and S (1.50 fold, p = 0.012) in the BCP group

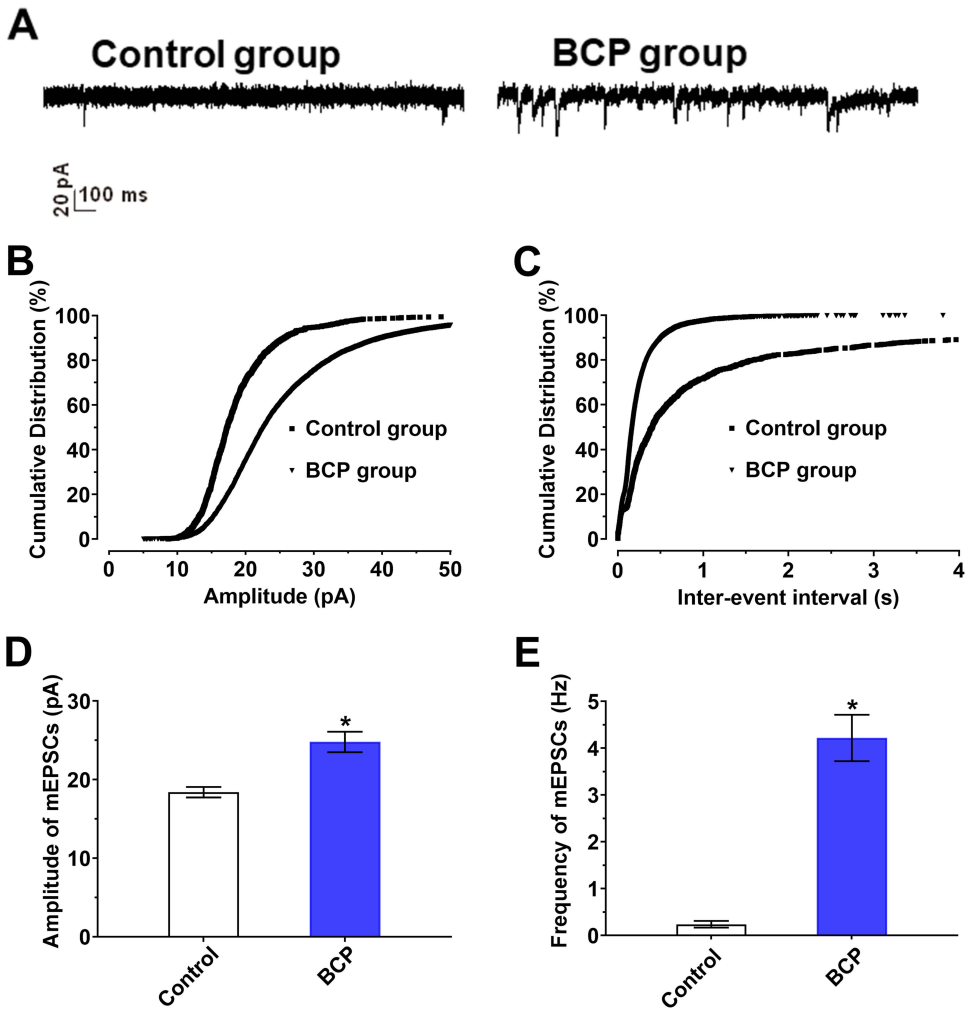

Figure 2 Ipsilateral spinal cord neuronal excitatory synaptic transmission. The waveforms (**A**), the cumulative distribution curves of amplitude (**B**) and inter-event interval (**C**) of mEPSCs were changed in the BCP group of rats, compared to the sham control group. The histograms of amplitude and frequency of mEPSCs were plotted, respectively (**D** and **E**) (n = 3, **p*<0.05).

of rats were significantly increased, while there were no significant changes in the other four macroelements, compared to the sham group, as shown in Figure 3.

For other twelve microelements, inoculation of Walker 256 cancer cells into the left tibia of rats drastically promoted the elevation of the content of the four elements (Fe [2.01 fold, $p = 0.038$], Mn [1.37 fold, $p = 0.005$], Li [4.91 fold, $p = 0.042$] and Sr [1.54 fold, $p = 0.016$]), compared to the control, as shown in Figure 4. In contrast, there were no significant changes in the other eight micro elements (Cu, Zn, Se, Si, Cr, Ni, Sn and Mo) (data not shown).

Among the other five toxic elements, the spinal cord level of the element Ti ($p = 0.017$) in the BCP group of rats was significantly 1.40-fold higher than that in the sham control group, as shown in Figure 5. There were no outstanding alterations in the other four elements (Al, As, Ba and Pb) between the sham control and BCP groups. In addition, 15 trace elements, including Ag, Be, Bi, Cd, Co, Ga, V, B, Ge, Sb, Re, Zr, Y, Nd and Gd, could not yet be detected, under the current monitoring conditions.

Correlation Coefficients and Patterns Among 23 Detected Elements in the Sham Control and BCP Groups of Rats

To further decipher relationship between elements in the spinal cord of the control and BCP groups of rats, the correlations between elements were calculated, according to the detected data above of the elemental contents in the

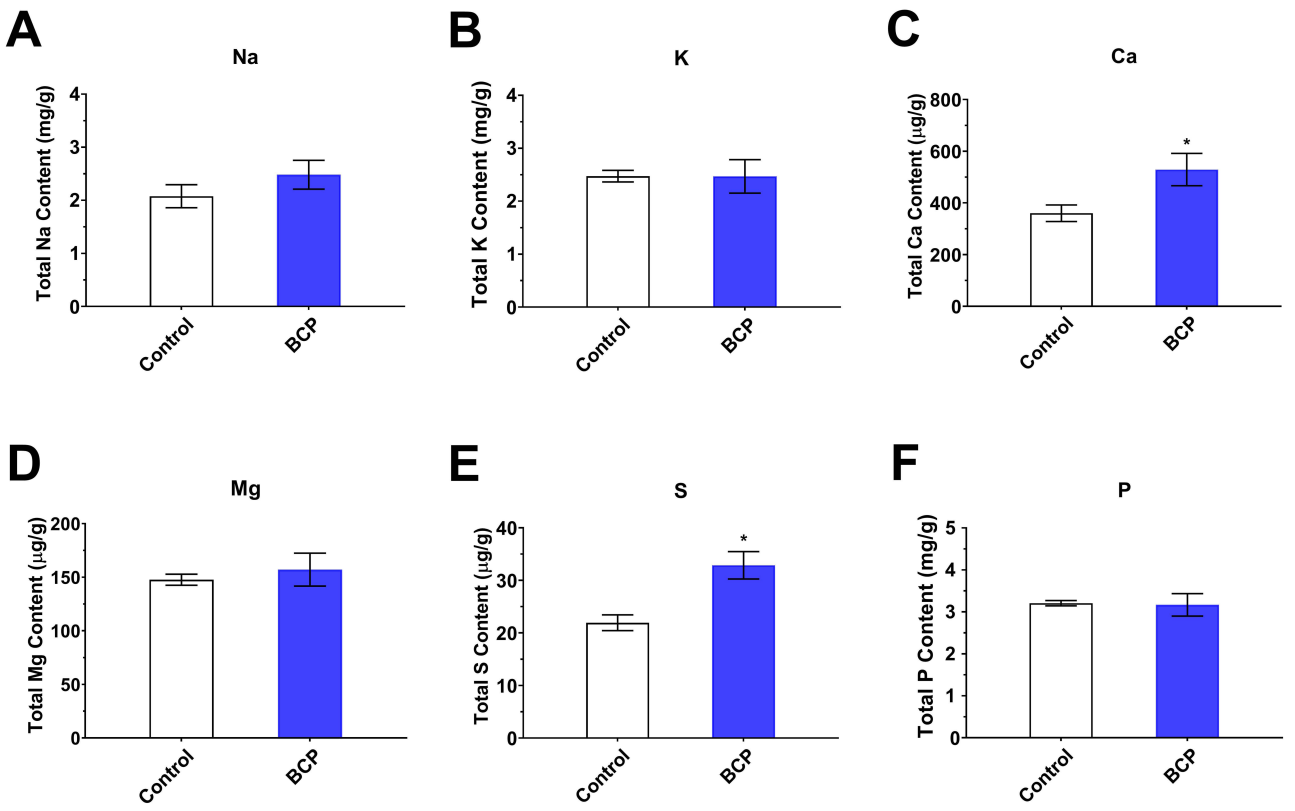

Figure 3 Changes in the contents of six macroelements (Na, K, Ca, Mg, S and P) between the sham control and BCP groups of rats (**A**–**F**). Significant alterations are denoted with an asterisk (n = 3–5, *p<0.05).

spinal cord. As shown in Table 1, many positive correlations were acquired, i.e., 39 and 47 for the sham control and BCP groups, respectively. Significantly negative correlations were also observed among all of the detected elements in the two groups of rats, i.e., 1 and 8, respectively. The strongest positive correlation was observed between the elements K-Mg (r = 0.998) in the BCP group, while that of the sham control group was Ca-Sr (r = 0.997). The strongest negative correlation was between the elements Na-P (r = −0.994) in the BCP group. These interesting data indicate that there is a close linkage between ionome and BCP and the metabolisms of ionome are involved into BCP.

To further explore changes in different categories of correlation patterns, we provide the positive correlation styles among the 23 detected elements, which are summarized in Table 2. There was an increase in the number of significant positive correlations for the macro-macro, macro-micro, macro-toxic and micro-micro categories in the BCP group, from 1, 8, 1, 11 to 3, 16, 3, 14, respectively, compared to the sham control group. The maximum type of significant positive correlations was the micro-toxic category with 15 in the sham control group and the macro-micro category with 16 in the BCP group. In contrast, for the micro-toxic category, the number of significant negative correlations was decreased from 15 to 8. These data suggest that the balance between macro-micro elements is more crucial than other types of correlation patterns of elements.

Changes in Patterns of Ionomic Profiles Between the Sham Control and BCP Model Rats

Finally, PCA was used to explore effects of BCP induced by inoculation of Walker 256 cancer cells into the left tibia on the ionomic patterns of the spinal cord in the study. Two major principal components were analyzed, with total variances of 44% and 23.60% for PC1 and PC2, respectively, as shown in Figure 6. PCA revealed significant differentiation between the sham control and BCP groups, suggesting that the patterns of ionomic profiles in the spinal cord of BCP model rats were completely different from that of control rats.

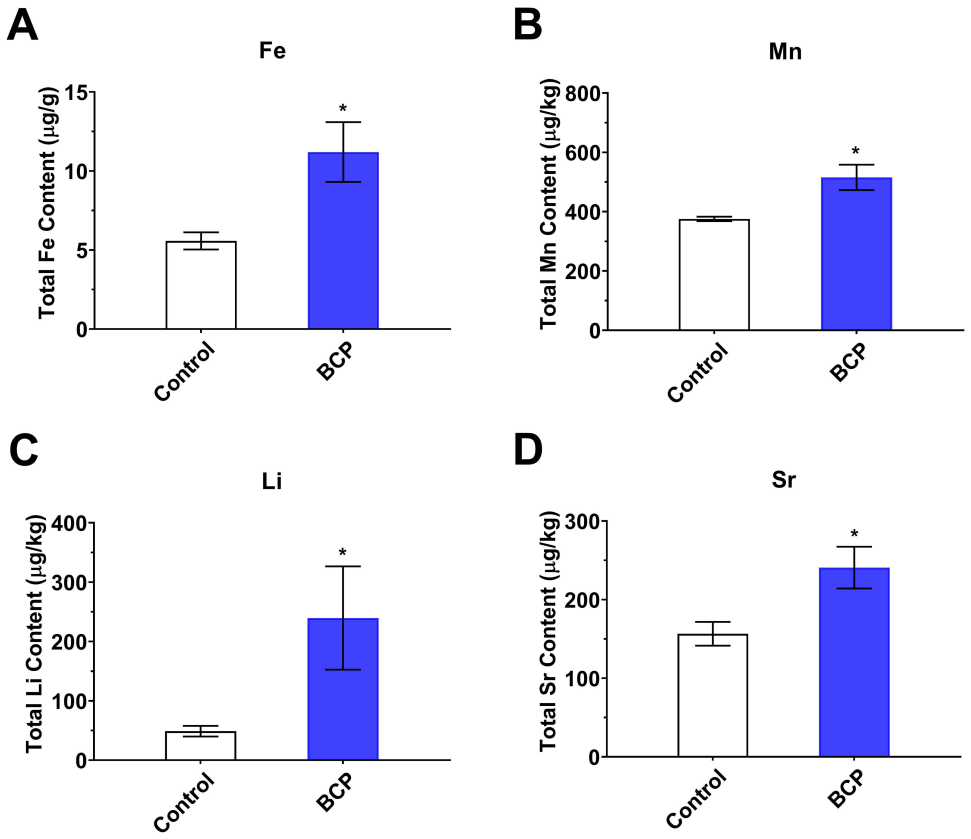

Figure 4 Changes in the contents of four microelements (Fe, Mn, Li and Sr) in the sham control and BCP groups of rats (**A**–**D**). Significant changes are denoted with an asterisk (n = 3–5, *p<0.05).

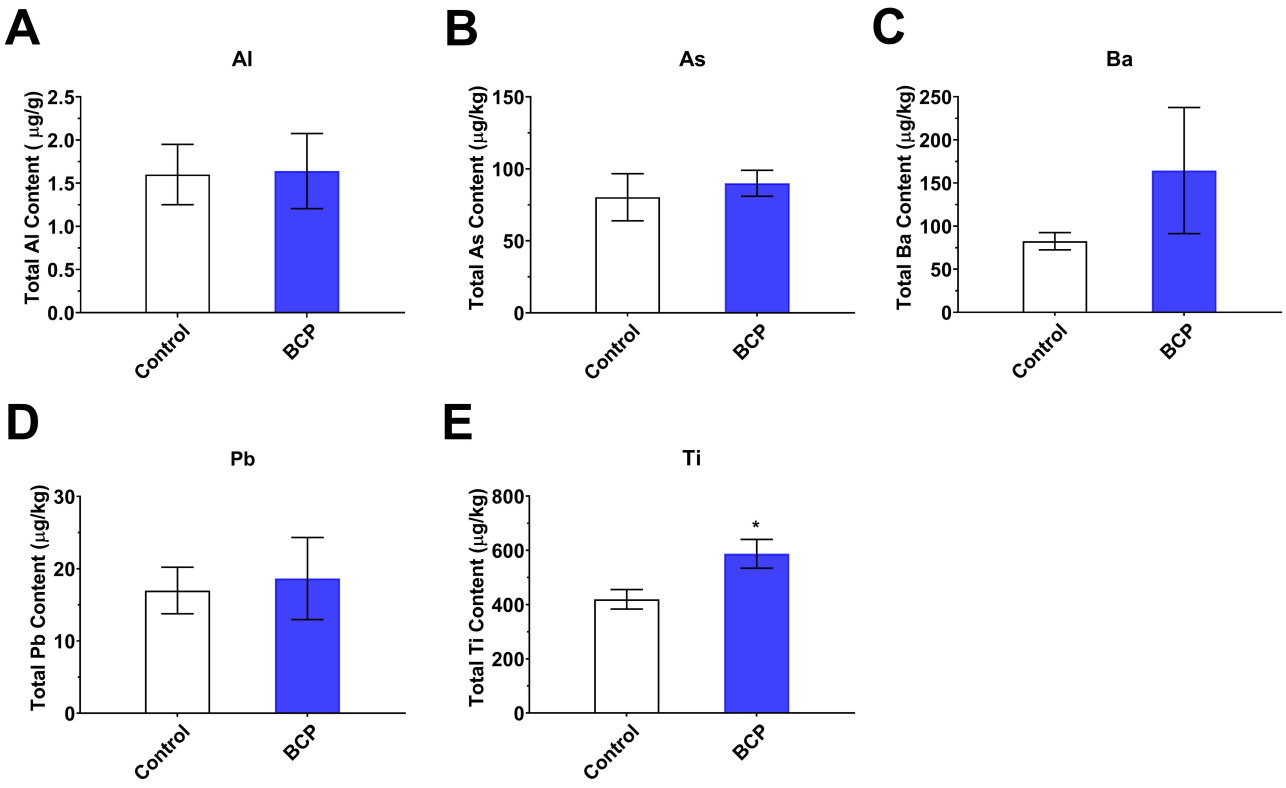

Figure 5 Changes in the toxic elemental contents (Al, As, Ba, Pb and Ti) between the sham control and BCP groups of rats (**A**–**E**). Significant changes are denoted with an asterisk (n = 3–5, *p<0.05).

Table 1 Correlation Coefficient Matrix for Detected Ionomic Profiles of the Spinal Cord in the Sham Control and BCP Groups of Rats, as Shown Below and Above the Diagonal, Respectively

	Na	K	Ca	Mg	S	P	Fe	Cu	Zn	Se	Si	Cr	Mn	Ni	Sn	Li	Mo	Sr	Al	As	Ba	Pb	Ti
Na		−0.988**	−0.668	−0.982**	−0.495	−0.994**	−0.226	−0.950*	−0.934*	−0.977**	−0.530	−0.809	−0.741	−0.504	−0.594	−0.567	−0.959**	−0.828	−0.574	−0.928*	−0.623	−0.490	−0.839
K	−0.755		0.645	0.998**	0.600	0.993**	0.249	0.962**	0.974**	0.965**	0.619	0.853	0.688	0.491	0.689	0.538	0.988**	0.805	0.580	0.877	0.604	0.509	0.833
Ca	−0.512	0.617		0.692	−0.010	0.733	0.411	0.370	0.647	0.722	−0.078	0.106	−0.049	−0.333	0.051	−0.525	0.643	0.970*	−0.286	0.894	−0.163	−0.108	0.959*
Mg	−0.356	0.831	0.698		0.595	0.994**	0.287	0.945*	0.981**	0.962**	0.609	0.837	0.560	0.440	0.683	0.477	0.991**	0.838	0.533	0.880*	0.557	0.469	0.867
S	−0.228	0.714	0.800	0.955*		0.522	0.277	0.652	0.714	0.534	0.987**	0.880*	−0.510	0.425	0.993**	0.324	0.684	0.130	0.573	0.182	0.395	0.431	0.227
P	−0.118	0.735	0.427	0.861	0.773		0.298	0.933*	0.960**	0.979**	0.550	0.808	0.567	0.428	0.617	0.477	0.977**	0.872	0.510	0.926*	0.551	0.434	0.891
Fe	−0.676	0.051	−0.077	−0.371	−0.497	−0.040		0.036	0.395	0.405	0.335	0.283	−0.934	−0.575	0.274	−0.503	0.364	0.249	−0.453	0.335	−0.537	−0.654	0.302
Cu	0.143	0.334	0.616	0.795	0.968*	0.605	−0.664		0.911*	0.903*	0.670	0.893*	0.997*	0.708	0.736	0.781	0.934*	0.582	0.781	0.770	0.789	0.705	0.610
Zn	−0.442	0.686	0.798	0.884*	0.981*	0.525	−0.647	0.812		0.938*	0.722	0.883*	0.142	0.369	0.785	0.374	0.997**	0.779	0.490	0.802	0.470	0.403	0.830
Se	−0.942*	0.729	0.300	0.235	−0.185	0.161	0.796	−0.357	0.191		0.591	0.841	0.478	0.399	0.625	0.467	0.960**	0.859	0.488	0.923*	0.507	0.341	0.888
Si	−0.646	0.740	0.633	0.775	0.913	0.380	−0.773	0.564	0.925*	0.424		0.918*	−0.494	0.442	0.986**	0.362	0.701	0.058	0.587	0.237	0.409	0.395	0.158
Cr	0.194	0.407	0.409	0.834	0.953*	0.759	−0.658	0.937*	0.722	−0.322	0.521		0.098	0.594	0.926*	0.615	0.888*	0.292	0.716	0.572	0.616	0.525	0.371
Mn	−0.116	0.595	−0.085	0.652	0.857	0.962*	0.455	0.181	−0.008	0.387	0.003	0.906		0.828	−0.437	0.876	0.379	0.137	0.776	0.448	0.921	0.915	0.060
Ni	0.215	0.253	0.609	0.737	0.957*	0.563	−0.643	0.994**	0.760	−0.429	0.484	0.911*	−0.194		0.474	0.988*	0.414	−0.099	0.985**	0.251	0.983**	0.942*	−0.097
Sn	0.168	0.287	0.550	0.762	0.937	0.545	−0.753	0.992**	0.809	−0.394	0.586	0.937*	−0.225	0.982**		0.425	0.761	0.204	0.619	0.292	0.462	0.477	0.297
Li	−0.558	0.824	−0.065	0.628	0.377	0.809	−0.040	0.207	0.279	0.573	0.440	0.518	0.946	0.129	0.195		0.438	−0.358	0.988*	0.368	0.994**	0.943	−0.429
Mo	0.057	0.437	0.679	0.855	0.990**	0.681	−0.578	0.992**	0.839	−0.257	0.593	0.936*	0.443	0.981**	0.971**	0.268		0.785	0.525	0.835	0.516	0.430	0.831
Sr	−0.818	0.603	0.997**	0.548	0.504	0.150	0.884	0.924	0.764	0.735	0.568	−0.284	−0.127	0.843	0.395	−0.339	0.829		−0.046	0.957*	0.072	0.133	0.994**
Al	−0.046	0.482	0.578	0.864	0.942	0.609	−0.755	0.952*	0.904*	−0.175	0.758	0.932*	0.193	0.914*	0.966**	0.345	0.948*	0.359		0.292	0.969**	0.932*	−0.026
As	−0.797	0.646	0.746	0.563	0.899	0.113	−0.635	0.359	0.820	0.553	0.904*	0.199	−0.252	0.300	0.363	−0.044	0.396	0.793	0.515		0.401	0.221	0.927
Ba	−0.129	0.510	0.498	0.839	0.883	0.548	−0.823	0.875	0.905*	−0.091	0.831	0.881*	0.118	0.821	0.907*	0.397	0.867	0.188	0.980**	0.574		0.949*	0.066
Pb	0.160	0.230	0.311	0.671	0.791	0.413	−0.920	0.880*	0.759	−0.380	0.649	0.886*	−0.146	0.846	0.930*	0.268	0.836	−0.331	0.942*	0.364	0.951*		0.137
Ti	−0.538	0.711	0.975**	0.819	0.923	0.518	−0.257	0.703	0.908*	0.315	0.775	0.542	−0.001	0.675	0.653	0.108	0.762	0.980*	0.716	0.808	0.664	0.471	

Note: Significant positive and negative correlations are marked with one or two asterisks (n = 3–5, *p<0.05, **p<0.01).

https://doi.org/10.2147/JPR.S447282 DovePress

Table 2 Changes in Correlation Patterns of Elements in the Spinal Cord of the Sham Control and BCP Groups of Rats (n = 3–5)

Type of Correlation	Control Group		BCP Group	
	No.[a]	Element-Element	No.[a]	Element-Element
Macro-Macro	1	S-Mg	3	K-Mg, K-P, Mg-P
Macro-Micro	8	Ca-Sr, Mg-Zn, S-Cu, S-Zn, S-Cr, S-Ni, S-Mo, P-Mn	16	K-Cu, K-Zn, K-Se, K-Mo, Ca-Sr, Mg-Cu, Mg-Zn, Mg-Se, Mg-Mo, S-Si, S-Cr, S-Sn, P-Cu, P-Zn, P-Se, P-Mo
Macro-Toxic	1	Ca-Ti	3	Ca-Ti, Mg-As, P-As
Micro-Micro	11	Cr-Cu, Ni-Cu, Sn-Cu, Mo-Cu, Si-Zn, Ni-Cr, Sn-Cr, Mo-Cr, Sn-Ni, Mo-Ni, Mo-Sn	14	Cu-Zn, Cu-Se, Zn-Se, Cu-Cr, Zn-Cr, Si-Cr, Cu-Mn, Si-Sn, Cr-Sn, Ni-Li, Cu-Mo, Zn-Mo, Se-Mo, Cr-Mo
Micro-Toxic	15	Cu-Al, Cu-Pb, Zn-Al, Zn-Ba, Zn-Ti, Si-As, Cr-Al, Cr-Ba, Cr-Pb, Ni-Al, Sn-Al, Sn-Ba, Sn-Pb, Mo-Al, Sr-Ti	8	Ni-Al, Li-Al, Se-As, Sr-As, Ni-Ba, Li-Ba, Ni-Pb, Sr-Ti
Toxic-Toxic	3	Ba-Al, Pb-Al, Pb-Ba	3	Ba-Al, Pb-Al, Pb-Ba

Note: [a]Total number of significant positive correlation between two elements.

Discussion

In the study, we explored changes in the ionomic profiles of the spinal cord and the correlations between elements, following behavioral and electrophysiological traits, in the rats with BCP compared to the control with sham operation. Algesic phenotypes of rats were demonstrated by mechanical nociceptive threshold testing and patch-clamp recordings. In agreement with our previous findings and others,[12,37] the ipsilateral PWTs of the group of rats bearing Walker 256 cancer cells gradually decreased over time in the 14-day observation period after surgery. In contrast, the ipsilateral PWTs of the sham control group of rats did not significantly change. The ipsilateral PWTs of BCP model rats were very low upon the 14th day in the study. It is

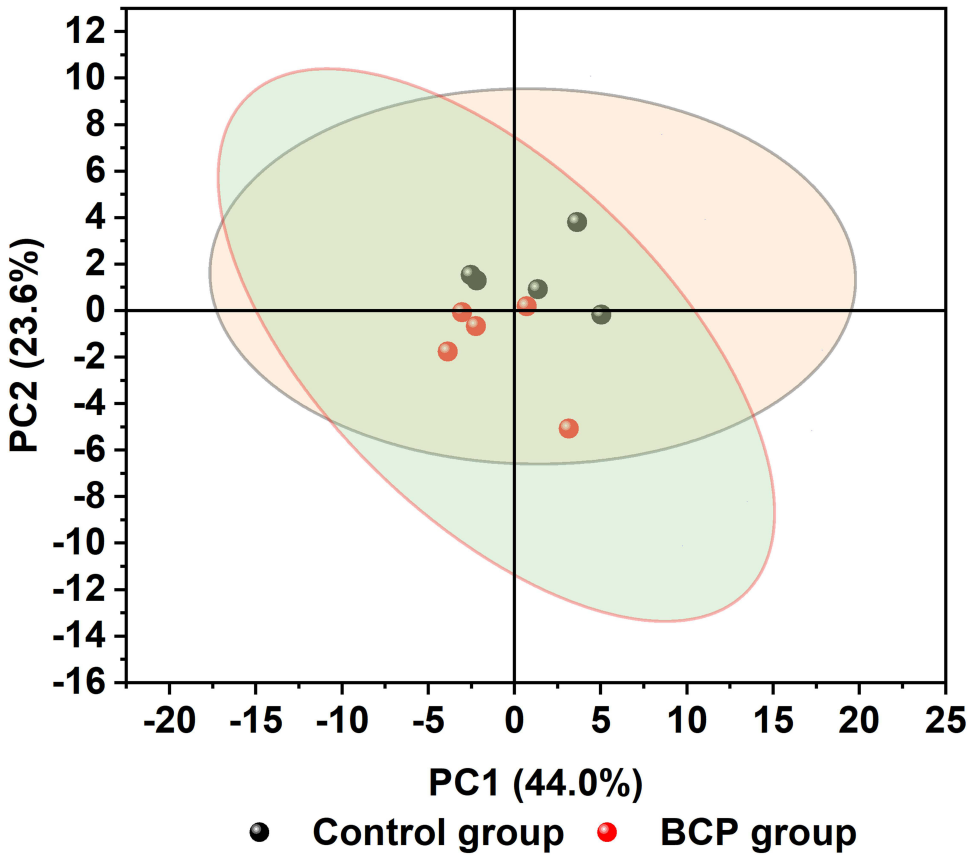

Figure 6 PCA biplot of the detected elemental levels of the spinal cord in the sham control and BCP group of rats is plotted as black and red dots, respectively (n=5). The PCA was performed with an enhanced version (v1.50) of PCA tool of the software Origin 2021.

considered to be hypersensitive to mechanical stimuli, as described in our and other previous studies.[12,38] Therefore, the time point on the 14th day was chosen to terminate the behavioral testing and conduct further study. By day 14, obvious enlargement of the ipsilateral tibiae was observed in the BCP model rats, in comparison to both the sham control rats and the contralateral ones of the model rats. The ipsilateral tibial swelling was considered to be markers of tumor growth and its erosion of bone tissues, which were indicative of hyperalgesia/allodynia as described in our and other previous studies.[12,39,40] Taken together, this result revealed that the rats with cancer cells progressively exhibited tumor-induced mechanical pain behavior, indicating that the rat model with BCP was successfully established.

Like the behavioral changes of the BCP rats, the neuro-electro-chemical and synaptic reorganization also deeply occurred in their spinal cords. Additionally, the balance of excitatory and inhibitory signaling closely linked to hyperalgesia was seriously disrupted in the spinal cord, such as releases of increased glutamate and decreased glycine. The imbalance between them dramatically promoted firing activities of spinal neurons and obviously caused alterations of spinal neuroplasticity under pain states.[41] The phenomenon of abnormal neuronal discharge has been demonstrated in many pain models, including spared nerve injury (SNI)-,[42] chronic constriction injury (CCI)-,[43] L5/L6 spinal nerve ligation (SNL)-induced neuropathic pain, and formalin-induced inflammatory pain.[44] Our present results suggested that the accumulative frequency and amplitude of mEPSCs in spinal dorsal horn neurons were strikingly strengthened in BCP model rats, compared to the sham control. With another femur BCP model in mice, Takasu et al recorded the enhancement of miniature inhibitory postsynaptic currents (mIPSCs) frequency.[45] It was understood that implantation of cancer cells into bones could trigger phenotypic alterations in both peripheral[46] and central nervous neurons. Therefore, these data collectively displayed that abnormal discharge activity of spinal cord neurons is also a phenotypic characteristic of BCP.

It is well reported that inorganic mineral elements are implicated in some important biological functions, due to their unique properties, such as maintaining antioxidant and immune activities.[47,48] Nonessential minerals, especially heavy metals (e.g., Pb, Cd and As), may cause diseases because they can become toxic when overloaded. On one hand, it is considerably important for elemental homeostasis in vivo to achieve human health. On the other hand, its dyshomeostasis may also have an influence on the complex networks of genes or proteins involved in varieties of pathophysiological processes. It is well known that there are close relationships between the contents of mineral elements and human diseases or longevity.[34,49,50] Interestingly, it has been demonstrated that there are direct or indirect correlation between a certain element and hyperalgesia/allodynia.[24,51–54] For example, Zn, an essential microelement which is widely present in the nervous system, can modulate the activities of functional proteins, such as metallopeptidase and metalloproteins.[54] Chronic Zn deficiency increases inflammation, decreases immunity and promote pain,[51,55] while complementary Zn attenuates thermal hyperalgesia.[52] The evidence above indicates a potential relationship between Zn and hyperalgesia. Another example which has recently been illustrated is that ferroptosis, a novel iron element-dependent manner of cell death, is involved in inflammation, neuropathic pain, allodynia and morphine tolerance,[19,26–28] suggesting the element iron plays critical roles in the process of pain. The third example is that Se is an important component of some enzymes in vivo,[56] and a biomarker of oxidative stress.[57] Previous findings revealed that Se mediated protective effects against docetaxel-induced adverse peripheral oxidative neurotoxicity and neuropathic pain in mice.[47] Yüksel et al reported that Se treatment significantly decreased fibromyalgia through modulating activities of TRPM2 and TRPV1 channels in rats.[48] Taken together, a certain element acting as a type of micronutrient exerts anti-nociceptive effects. In a line with the results above, contents of many elements in spinal cords of rats were significantly changed by BCP, indicating they were closely participated into BCP in the study.

The concept of ionome was first proposed by Lahner et al twenty years ago.[31] It represents the inorganic components of cellular and organismal systems and provides a very effective tool for not only identifying new knowledge of element metabolism and homeostasis but also gaining more information about how the complex ionomic network is affected by different factors. Ionomic technologies, such as ICP-MS, can measure and quantify elemental profiles to further analyze their variation. It has been applied into different tissue samples, such as canine hairs exposed to lipopolysaccharide (LPS)-induced stress,[58] pericardial fluid in ischemic heart disease,[59] and blood.[32] In the study, the ICP-MS technology was applied to test ionome levels in the spinal cord samples. And the contents of a group of 23 micro-nutritional elements were detected in both groups of rats. Not only six macroelements (Na, K, Ca, Mg, P and S), but also twelve microelements (Fe, Zn, Cu, Mn, Se et al) and other five toxic elements (Al, As, Ba, Pb and Ti)[58,60] were detected. Many micronutrients are essential cofactors needed only in small amounts for functions of cells. Herein, characteristic ionomic profiles of the spinal cords from both the sham

control and BCP groups of rats were identified and comprehensively analyzed. Our data revealed that, compared to the sham control group, some microtrophic elements was differentially changed in the BCP group, suggesting that the spinal cord ionome was closely associated to BCP and implying a highly dynamic and complex crosstalk among these elements.[34] However, the sources of those toxic elements and the mechanisms of Ti accumulation in the spinal cord are still unclear. One possible explanation is that increased metabolism in rats with BCP leads to certain micronutriental dysfunction in some metabolic process and an accumulation of toxic ions throughout the body including the spinal cord. Similarly, accumulated Al in the dorsal root ganglia or other organs aggravated oxaliplatin-induced neuropathic pain in mice, which was alleviated by the chelation action of glutathione on Al.[61] Therefore, changes in elemental levels in the spinal cord from rats might contribute to the development of BCP.

Loss of function or gain of function of element-dependent proteins could positively or negatively affect metabolisms of other elements in some particular manners.[18] The opinion was partly supported by the findings that ceruloplasmin, a copper-dependent protein, strictly regulated iron metabolism, which was firstly discovered by Guan et al.[62] Indeed, intramuscular injection of lipopolysaccharide (LPS) in canines shifted correlation patterns between elements of their hair samples.[58] Based on these findings, it is agreed that some interactions between elements should be examined as a whole system or ionome. A growing body of evidence exhibits that abnormalities of the mineral metabolism can cause the specific dysfunctions of the nervous system.[63] In the elemental correlation analysis of spinal cords, the number of significant positive and negative correlation in the BCP group was more than that in the sham control group, suggesting that the balance between elements was disrupted. The current data manifested that BCP is closely associated with imbalance of elements. In previous studies, the positive correlation between Ca and Mg was well documented.[58,64] In the study, the Ca-Mg correlation was not significant, while the Mg-K positive correlation ($r = 0.998$) in the BCP group was sharply higher than that in the sham control group. Conversely, it was shown that the Ca-Sr correlation was greatly decreased in the BCP group, in contrast to the sham control group. Subsequently, element interactions may modulate their contribution to BCP. And changes in ionome can be mapped back to sequence variation in the genome and may also reflect broader biologically relevant disorders.[18] It was demonstrated, for the first time, that the correlation pattern of the ionome of the spinal cord of the BCP model rats was exceptionally different from that of the sham control in the study. The PCA analysis also revealed that mineral profiles of the spinal cord samples between the two groups of rats were significantly divergent. Overall, significant correlation of all tested elements and their changes were observed in the study.

Conclusions

The findings indicated that spinal cord ionome may be a related factor of BCP, which expand our understanding of the pathogenesis on BCP. Analyzing the multivariate data and elemental distribution patterns provided novel available information, i.e., the BCP may be strongly impacted by alterations of the ionomic profiles of the spinal cord. The element correlation networks have been clearly built in the study. Anyway, roles of ionome under hyperalgesic conditions have attracted our attention. Further studies are recommended for exploring the mechanism of the imbalance of element metabolism in the pathological process of BCP in rats. A new research field was opened up, and it may ultimately be beneficial in devising interventions to prevent and treat BCP.

Ethical Approval

All procedures performed in the study involving animals were in accordance with an approved protocol issued by Animal Care and Welfare Committee of Shanghai Municipal Sixth People's Hospital, Shanghai, China. The animal experiments strictly adhered to the National Institutes of Health Guide for Care and Use of Laboratory Animals (Publication No. 80-23, revised 1996). The use of Walker 256 cells in the study was approved by the Research Ethics Committee of Shanghai Municipal Sixth People's Hospital.

Acknowledgments

The authors would like to thank Prof. Ling Xu at LongHua Hospital Shanghai University of Traditional Chinese Medicine, Shanghai, China, for the kind gift of Walker 256 cancer cell line. We also would like to thank Master Zhanying Wei from

Department of Osteoporosis and Bone Diseases, Shanghai Sixth People's Hospital Affiliated to Shanghai Jiao Tong University School of Medicine, for the μCT scan experimental assistance.

Funding

This work was partially supported by the National Natural Science Foundation of China (81603082), Shanghai "Rising Stars of Medical Talent" Youth Development Program (Youth Medical Talents-Clinical Pharmacists Program).

Disclosure

The authors declare that they have no known competing financial interests or personal relationships that could have appeared to influence the work reported in this paper.

References

1. Xu L, Wang S, Zhang L, Liu B, Zheng S, Yao M. Cobratoxin alleviates cancer-induced bone pain in rats via inhibiting CaMKII signaling pathway after acting on M4 muscarinic cholinergic receptors. *ACS Chem Neurosci*. 2022;13(9):1422–1432. doi:10.1021/acschemneuro.2c00048
2. Wang K, Donnelly CR, Jiang C, et al. STING suppresses bone cancer pain via immune and neuronal modulation. *Nat Commun*. 2021;12:4558. doi:10.1038/s41467-021-24867-2
3. Snijders RAH, Brom L, Theunissen M, van den Beuken-van Everdingen MHJ. Update on prevalence of pain in patients with cancer 2022: a systematic literature review and meta-analysis. *Cancers*. 2023;15:591. doi:10.3390/cancers15030591
4. Huang JL, Guo C. Advances on bone cancer pain and its models. *Lett in Biotech*. 2020;31(2):214–219. doi:10.3969/j.issn.1009-0002.2020.02.015
5. Liang Y, Liu Y, Hou B, et al. CREB-regulated transcription coactivator 1 enhances CREB-dependent gene expression in spinal cord to maintain the bone cancer pain in mice. *Mol Pain*. 2016;12:1–11. doi:10.1177/1744806916641679
6. Shenoy PA, Kuo A, Leparc G, et al. Transcriptomic characterisation of the optimised rat model of Walker 256 breast cancer cell-induced bone pain. *Clin Exp Pharmacol Physiol*. 2019;46:1201–1215. doi:10.1111/1440-1681.13165
7. Wang A, Guo D, Cheng H, Jiang H, Liu X, Yun Z. Transcriptome sequencing explores the mechanism of Baicalin on bone cancer pain. *J Inflamm Res*. 2021;14:5999–6010. doi:10.2147/jir.S336028
8. Hou X, Weng Y, Guo Q, et al. Transcriptomic analysis of long noncoding RNAs and mRNAs expression profiles in the spinal cord of bone cancer pain rats. *Mol Brain*. 2020;13(47):1–16. doi:10.1186/s13041-020-00589-2
9. Romero-Morelos P, Ruvalcaba-Paredes E, Garciadiego-Cázares D, et al. Neurophysiological mechanisms related to pain management in bone tumors. *Curr Neuropharmacol*. 2021;19(3):308–319. doi:10.2174/1570159x18666201111112748
10. Diaz-delCastillo M, Christiansen SH, Appel CK, Falk S, Woldbye DPD, Heegaard A-M. Neuropeptide Y is up-regulated and induces antinociception in cancer-induced bone pain. *Neuroscience*. 2018;384:111–119. doi:10.1016/j.neuroscience.2018.05.025
11. Zhao J, Yan Y, Zhen S, et al. LY294002 alleviates bone cancer pain by reducing mitochondrial dysfunction and the inflammatory response. *Int J Mol Med*. 2023;51(42):1–12. doi:10.3892/ijmm.2023.5245
12. Huang JL, Chen XL, Guo C, Wang YX. Contributions of spinal D-amino acid oxidase to bone cancer pain. *Amino Acids*. 2012;43(5):1905–1918. doi:10.1007/s00726-012-1390-z
13. Zhang JY, Gong N, Huang JL, Guo LC, Wang YX. Gelsemine, a principal alkaloid from Gelsemium sempervirens Ait., exhibits potent and specific antinociception in chronic pain by acting at spinal α3 glycine receptors. *Pain*. 2013;154(11):2452–2462. doi:10.1016/j.pain.2013.07.027
14. Zheng XQ, Wu YH, Huang JF, Wu AM. Neurophysiological mechanisms of cancer-induced bone pain. *J Adv Res*. 2022;35:117–127. doi:10.1016/j.jare.2021.06.006
15. Tansley S, Gu N, Guzmán AU, et al. Microglia-mediated degradation of perineuronal nets promotes pain. *Science*. 2022;377(6601):80–86. doi:10.1126/science.abl6773
16. Barkai O, Rayi PR, Butterman R, Katz B, Lev S, Binshtok AM. Encoding of inflammatory hyperalgesia in mouse spinal cord. *Pain*. 2023;164(2):443–460. doi:10.1097/j.pain.0000000000002727
17. Falk S, Dickenson AH. Pain and nociception: mechanisms of cancer-induced bone pain. *J Clin Oncol*. 2014;32(16):1647–1654. doi:10.1200/JCO.2013.51.7219
18. Fleet JC, Replogle R, Salt DE. Systems genetics of mineral metabolism. *J Nutr*. 2011;141(3):520–525. doi:10.3945/jn.110.128736
19. Dixon SJ, Lemberg KM, Lamprecht MR, et al. Ferroptosis: an iron-dependent form of nonapoptotic cell death. *Cell*. 2012;149(5):1060–1072. doi:10.1016/j.cell.2012.03.042
20. Tsvetkov P, Coy S, Petrova B, et al. Copper induces cell death by targeting lipoylated TCA cycle proteins. *Science*. 2022;375(6586):1254–1261. doi:10.1126/science.abf0529
21. Zhao G, Liu SJ, Gan XY, et al. Analysis of whole blood and urine trace elements in children with autism spectrum disorders and autistic behaviors. *Biol Trace Elem Res*. 2023;201(2):627–635. doi:10.1007/s12011-022-03197-4
22. Zheng L, Zhu HZ, Wang BT, et al. Sodium selenate regulates the brain ionome in a transgenic mouse model of Alzheimer's disease. *Sci Rep*. 2016;6:39290. doi:10.1038/srep39290
23. Dubey P, Thakur V, Chattopadhyay M. Role of minerals and trace elements in diabetes and insulin resistance. *Nutrients*. 2020;12(6):1864. doi:10.3390/nu12061864
24. Mert T, Gunes Y, Ozcengiz D, Gunay I. Magnesium modifies fentanyl-induced local antinociception and hyperalgesia. *Naunyn-Schmied Arch Pharmacol*. 2009;380(5):415–420. doi:10.1007/s00210-009-0447-3
25. Tomita S, Sekiguchi F, Naoe K, et al. $Ca_v3.2$-dependent hyperalgesia/allodynia following intrathecal and intraplantar zinc chelator administration in rodents. *J Pharmacol Sci*. 2023;152(2):86–89. doi:10.1016/j.jphs.2023.03.007

26. Li S, Zhou C, Zhu Y, et al. Ferrostatin-1 alleviates angiotensin II (Ang II)- induced inflammation and ferroptosis in astrocytes. *Int Immunopharmacol*. 2021;90:107179. doi:10.1016/j.intimp.2020.107179
27. Wang H, Huo X, Han C, et al. Ferroptosis is involved in the development of neuropathic pain and allodynia. *Mol Cell Biochem*. 2021;476 (8):3149–3161. doi:10.1007/s11010-021-04138-w
28. Chen X, Zhang B, Liu T, et al. Liproxstatin-1 attenuates morphine tolerance through inhibiting spinal ferroptosis-like cell death. *ACS Chem Neurosci*. 2019;10(12):4824–4833. doi:10.1021/acschemneuro.9b00539
29. Filipiak M, Filipiak ZM. Application of ionomics and ecological stoichiometry in conservation biology: nutrient demand and supply in a changing environment. *Biol Conserv*. 2022;272:109622. doi:10.1016/j.biocon.2022.109622
30. Salt DE, Baxter I, Lahner B. Ionomics and the study of the plant ionome. *Annu Rev Plant Biol*. 2008;59:709–733. doi:10.1146/annurev.arplant.59.032607.092942
31. Lahner B, Gong J, Mahmoudian M, et al. Genomic scale profiling of nutrient and trace elements in Arabidopsis thaliana. *Nat Biotechnol*. 2003;21 (10):1215–1221. doi:10.1038/nbt865
32. Zhang Y, Huang B, Jin J, Xiao Y, Ying H. Recent advances in the application of ionomics in metabolic diseases. *Front Nutr*. 2023;9:1111933. doi:10.3389/fnut.2022.1111933
33. Silver MK, Arain AL, Shao J, et al. Distribution and predictors of 20 toxic and essential metals in the umbilical cord blood of Chinese newborns. *Chemosphere*. 2018;210:1167–1175. doi:10.1016/j.chemosphere.2018.07.124
34. Li Q, Hu C, Lin J, et al. Urinary ionomic analysis reveals new relationship between minerals and longevity in a Han Chinese population. *J Trace Elem Med Biol*. 2019;53:69–75. doi:10.1016/j.jtemb.2019.02.002
35. Ma L, Peng S, Wei J, et al. Spinal microglial β-endorphin signaling mediates IL-10 and exenatide-induced inhibition of synaptic plasticity in neuropathic pain. *CNS Neurosci Ther*. 2021;27(10):1157–1172. doi:10.1111/cns.13694
36. Gong N, Gao ZY, Wang YC, et al. A series of D-amino acid oxidase inhibitors specifically prevents and reverses formalin-induced tonic pain in rats. *J Pharmacol Exp Ther*. 2011;336(1):282–293. doi:10.1124/jpet.110.172353
37. Mao-Ying QL, Zhao J, Dong ZQ, et al. A rat model of bone cancer pain induced by intra-tibia inoculation of Walker 256 mammary gland carcinoma cells. *Biochem Biophys Res Commun*. 2006;345(4):1292–1298. doi:10.1016/j.bbrc.2006.04.186
38. Gu YJ, Qian HY, Zhou F, et al. Folic acid relieves bone cancer pain by downregulating P2X2/3 receptors in rats. *Brain Res*. 2023;1811:148405. doi:10.1016/j.brainres.2023.148405
39. Honore P, Luger NM, Sabino MA, et al. Osteoprotegerin blocks bone cancer-induced skeletal destruction, skeletal pain and pain-related neurochemical reorganization of the spinal cord. *Nat Med*. 2000;6(5):521–528. doi:10.1038/74999
40. Wang Y, Xu C, Liu P, et al. LncRNA 51325 alleviates bone cancer induced hyperalgesia through inhibition of Pum2. *J Pain Res*. 2024;17:265–284. doi:10.2147/jpr.S446635
41. Ma L, Ju P, Wang W, et al. Microglial activation of GLP-1R signaling in neuropathic pain promotes gene expression adaption involved in inflammatory responses. *Neural Plast*. 2021;2021:9923537. doi:10.1155/2021/9923537
42. Guida F, De Gregorio D, Palazzo E, et al. Behavioral, biochemical and electrophysiological changes in spared nerve injury model of neuropathic pain. *Int J Mol Sci*. 2020;21(9):3396. doi:10.3390/ijms21093396
43. Gabay E, Tal M. Pain behavior and nerve electrophysiology in the CCI model of neuropathic pain. *Pain*. 2004;110(1–2):354–360. doi:10.1016/j.pain.2004.04.021
44. Asante CO, Wallace VC, Dickenson AH. Formalin-induced behavioural hypersensitivity and neuronal hyperexcitability are mediated by rapid protein synthesis at the spinal level. *Mol Pain*. 2009;5:27. doi:10.1186/1744-8069-5-27
45. Takasu K, Ogawa K, Nakamura A, et al. Enhanced GABAergic synaptic transmission at VLPAG neurons and potent modulation by oxycodone in a bone cancer pain model. *Br J Pharmacol*. 2015;172(8):2148–2164. doi:10.1111/bph.13039
46. Zhu YF, Ungard R, Seidlitz E, et al. Differences in electrophysiological properties of functionally identified nociceptive sensory neurons in an animal model of cancer-induced bone pain. *Mol Pain*. 2016;12:1–14. doi:10.1177/1744806916628778
47. Ertilav K, Nazıroğlu M, Ataizi ZS, Yıldızhan K. Melatonin and selenium suppress docetaxel-induced TRPV1 activation, neuropathic pain and oxidative neurotoxicity in mice. *Biol Trace Elem Res*. 2021;199(4):1469–1487. doi:10.1007/s12011-020-02250-4
48. Yüksel E, Nazıroğlu M, Şahin M, Çiğ B. Involvement of TRPM2 and TRPV1 channels on hyperalgesia, apoptosis and oxidative stress in rat fibromyalgia model: protective role of selenium. *Sci Rep*. 2017;7(1):17543. doi:10.1038/s41598-017-17715-1
49. Shen Z, Lin J, Teng J, et al. Association of urinary ionomic profiles and acute kidney injury and mortality in patients after cardiac surgery. *J Thorac Cardiovasc Surg*. 2020;159(3):918–926.e5. doi:10.1016/j.jtcvs.2019.02.095
50. Bagher Pour O, Yahyavi Y, Karimi A, et al. Serum trace elements levels and clinical outcomes among Iranian COVID-19 patients. *Int J Infect Dis*. 2021;111:164–168. doi:10.1016/j.ijid.2021.08.053
51. Ozaki T, Matsuoka J, Tsubota M, et al. Zinc deficiency promotes cystitis-related bladder pain by enhancing function and expression of $Ca_v3.2$ in mice. *Toxicology*. 2018;393:102–112. doi:10.1016/j.tox.2017.11.012
52. Liu T, Walker JS, Tracey DJ. Zinc alleviates thermal hyperalgesia due to partial nerve injury. *Neuroreport*. 1999;10(3):645–649. doi:10.1097/00001756-199902250-00037
53. Ferraz CR, Carvalho TT, Fattori V, et al. Jararhagin, a snake venom metalloproteinase, induces mechanical hyperalgesia in mice with the neuroinflammatory contribution of spinal cord microglia and astrocytes. *Int J Biol Macromol*. 2021;179:610–619. doi:10.1016/j.ijbiomac.2021.02.178
54. Gomez R, Por ED, Berg KA, Clarke WP, Glucksman MJ, Jeske NA. Metallopeptidase inhibition potentiates bradykinin-induced hyperalgesia. *Pain*. 2011;152(7):1548–1554. doi:10.1016/j.pain.2011.02.044
55. Bonaventura P, Benedetti G, Albarède F, Miossec P. Zinc and its role in immunity and inflammation. *Autoimmun Rev*. 2015;14(4):277–285. doi:10.1016/j.autrev.2014.11.008
56. Nazıroğlu M, Öz A, Yıldızhan K. Selenium and neurological diseases: focus on peripheral pain and TRP channels. *Curr Neuropharmacol*. 2020;18 (6):501–517. doi:10.2174/1570159x18666200106152631
57. Dohrn MF, Dumke C, Hornemann T, et al. Deoxy-sphingolipids, oxidative stress, and vitamin C correlate with qualitative and quantitative patterns of small fiber dysfunction and degeneration. *Pain*. 2022;163(9):1800–1811. doi:10.1097/j.pain.0000000000002580

58. So KM, Lee Y, Bok JD, Kim EB, Chung MI. Analysis of ionomic profiles of canine hairs exposed to lipopolysaccharide (LPS)-induced stress. *Biol Trace Elem Res*. 2016;172(2):364–371. doi:10.1007/s12011-015-0611-1
59. Khan N, Hashmi S, Siddiqui AJ, et al. Ionomic profiling of pericardial fluid in ischemic heart disease. *RSC Adv*. 2020;10(60):36439–36451. doi:10.1039/d0ra03977b
60. Lee YH, Bang ES, Lee JH, et al. Serum concentrations of trace elements zinc, copper, selenium, and manganese in critically ill patients. *Biol Trace Elem Res*. 2019;188(2):316–325. doi:10.1007/s12011-018-1429-4
61. Lee M, Cho S, Roh K, et al. Glutathione alleviated peripheral neuropathy in oxaliplatin-treated mice by removing aluminum from dorsal root ganglia. *Am J Transl Res*. 2017;9(3):926–939.
62. Guan X, Bai X, Zhou C, et al. Serum ceruloplasmin depletion is associated with magnetic resonance evidence of widespread accumulation of brain iron in Parkinson's disease. *J Magn Reson Imaging*. 2021;54(4):1098–1106. doi:10.1002/jmri.27680
63. Wandt VK, Winkelbeiner N, Bornhorst J, et al. A matter of concern - Trace element dyshomeostasis and genomic stability in neurons. *Redox Biol*. 2021;41:101877. doi:10.1016/j.redox.2021.101877
64. Pasha Q, Malik SA, Iqbal J, Shah MH. Characterization and distribution of the selected metals in the scalp hair of cancer patients in comparison with normal donors. *Biol Trace Elem Res*. 2007;118(3):207–216. doi:10.1007/s12011-007-0035-7